3.1 COMPARISON OF ANGULAR DEPENDENCE OF OBSERVED AND SIMULATED DISTRIBUTIONS OF RADIANCES OVER STRATOCUMULUS CLOUDS

Mikhail Ovtchinnikov* and Roger Marchand
Pacific Northwest National Laboratory, Richland, Washington,

1. INTRODUCTION

In this study, we use multiangular radiance distributions measured by the AirMISR – the airborne version of Multiangle Imaging SpectroRadiometer (MISR) – to evaluate the structure of continental stratocumulus simulated by a high-resolution cloud resolving model. While the CRM cannot be expected to reproduce any particular cloud scene exactly, the observed and simulated cloud fields should have the same statistical properties. By comparing the statistics of the simulated radiance fields with the statistics of the actual AirMISR measurements we aim to ascertain the fidelity of the high-resolution cloud model. Establishing realism of the simulated cloud and radiance fields is necessary in justifying using such simulations as surrogates for developing and testing conceptual models, retrieval algorithms, and parameterizations.

2. OBSERVATIONS

On March 3, 2000, low and middle level clouds formed over the Atmospheric Radiation Measurement program (ARM) Southern Great Plains (SGP) site in the wake of a cold front. As part of the EOS validation campaign and ARM cloud IOP, ground remote sensing observations and aircraft measurements (both in and above clouds) were coordinated with Terra overpass. By 17:39 UTC, the time of Terra satellite overpass, the middle-level clouds had drifted away and the ARM site was covered by single-layer low clouds. The NASA high altitude ER-2 aircraft carrying AirMISR on board overflew the SGP Central Facility (CF) site (36.607N, 97.488W) at 17:39:10 UTC. It takes about nine minutes for AirMISR to image any location from all nine MISR-like view angles. Unlike MISR, which has a separate camera for each viewing angle (Diner et al., 2005), AirMISR uses a single turning camera taking subsequent snapshots of a scene at MISR's angles. Therefore, only one scene is sampled by AirMISR over the 17:33-17:45 UTC flight segment providing the angular distribution of radiances for only a relatively small region around the ARM central facility (on the order of 10×10 km^2). The benefit of using these data is in the much higher resolution (27.5 m) of the AirMISR imagery compared to the MISR imagery (275 m), which is, of course, a direct consequence of the lower flying altitude of ER-2 (20 km) compared to that of Terra (705 km).

* *Corresponding author address*: Mikhail Ovtchinnikov, Pacific Northwest National Laboratory, P.O.Box 999, Richland, WA 99352; e-mail:Mikhail@pnl.gov

3. CLOUD RESOLVING MODEL

The cloud resolving model used in this study is that of Khairoutdinov and Randall (2003). The model is run in a large-eddy simulation (LES) mode with a bulk treatment of the cloud microphysics. The model domain consists of 200×200×160 grid cells covering 5×5×3.2 km^3 physical domain with uniform 25-m horizontal and 20-m vertical resolutions. Periodic boundary conditions are used in both horizontal directions. In order to account for changes in the environment due to synoptic-scale circulation, which are important for simulations over several hours, prescribed tendencies are imposed on temperature and moisture fields and horizontal wind components are nudged toward observations. Latent and sensible surface heat fluxes are prescribed based on observations at the ARM SGP site. The forcing is the same as used in a recent model intercomparison study, which focused on simulating the frontal passage over the ARM central facility in north-central Oklahoma on 2-3 March 2000 (Xie et al., 2005). The simulation setup is different in that we run the model at much higher resolution on a smaller domain and for a shorter period of time, concentrating on the post-frontal low-level clouds. Our CRM simulation begins at 15:00 UTC and lasts for four hours. A snapshot of the cloud field at 18:00 UTC then serves as input to 3D radiation calculations described below.

4. 3-D RADIATIVE TRANSFER CALCULATIONS

Simulated radiances are obtained using the Spherical Harmonic Discrete Ordinate Method (SHDOM) radiation transfer (RT) code (Evans, 1998). SHDOM is run in full 3D mode with cyclic boundary conditions. Monochromatic radiances are computed for 0.443 μm wavelength (the blue AirMISR channel) for which molecular Rayleigh scattering is accounted for and gaseous absorption is neglected. The surface is treated as Lambertian with albedo of 0.04, based on spectral albedo measurements around the SGP site in March 2000. Spatial distribution of the cloud water is taken from the CRM. In computations of the extinction cross section, single scattering albedo, and phase function using Mie theory the droplet size spectrum is assumed to follow a gamma distribution with effective radius of 6.8 μm and effective variance of 0.1 (shape parameter of 7). The computational domain includes all layers containing liquid water plus two layers below the cloud base and five layers between the highest cloud top and 20 km. The geometry of the radiation simulation matches the AirMISR – Sun configuration. The solar zenith angle is set to 45 degrees and the solar

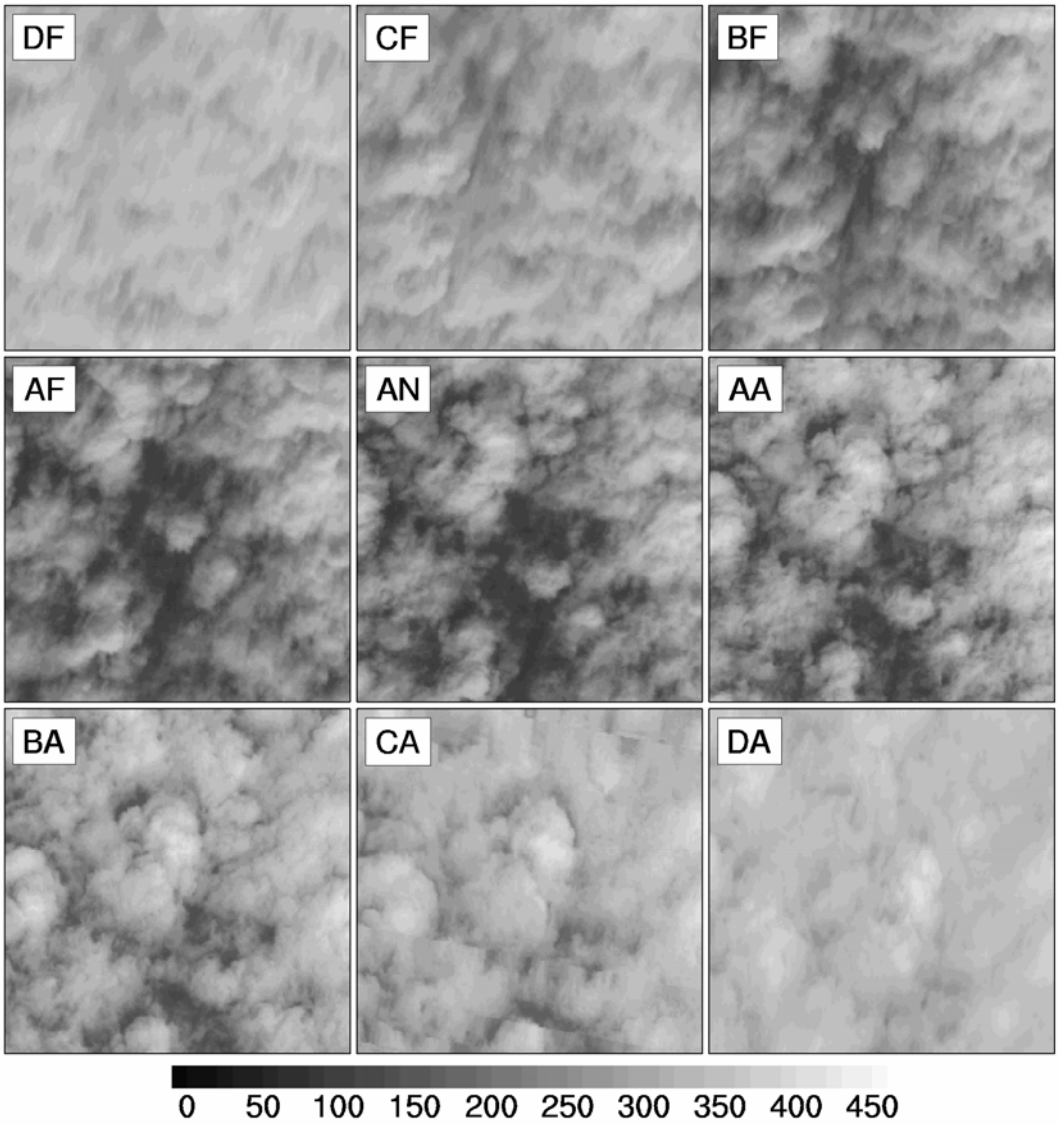

Figure 1. *Observed blue channel (λ=0.443 μm) radiances (W m^{-2} μm^{-1} sr^{-1}) for the nine AirMISR cameras listed in Table 1. Each panel consists of 200×200 pixels at 27.5 m resolution.*

azimuth is 105 degrees. The plane track is 36 degrees off the solar principle plane. Zenith and scattering angles corresponding to the nine AirMISR cameras are given in Table 1. In computing radiances for the nine camera angles we neglect the evolution of the cloud field and the change in Sun's position during the nine minutes it takes for the AirMISR to sample the study area.

Table 1. *Zenith and scattering angles for nine AirMISR cameras.*

Camera	Viewing direction	Viewing zenith angle, ξ (°)	Scattering angle, θ (°)
DF	fore	70.5	72.3
CF		60.0	81.8
BF		45.6	94.9
AF		26.1	112.5
AN	nadir	0	135.0
AA	aft	26.1	152.5
BA		45.6	154.6
CA		60.0	148.1
DA		70.5	140.8

4. RESULTS

Figures 1 and 2 show the observed and simulated radiances for nine viewing angles. The near nadir views (AF, AN, and AA camera angles) show cloud elements of similar horizontal size with dark ground seen in-between. Cloud gaps become progressively less visible as viewing angle increases and close nearly completely at the most oblique views (DF and DA cameras).

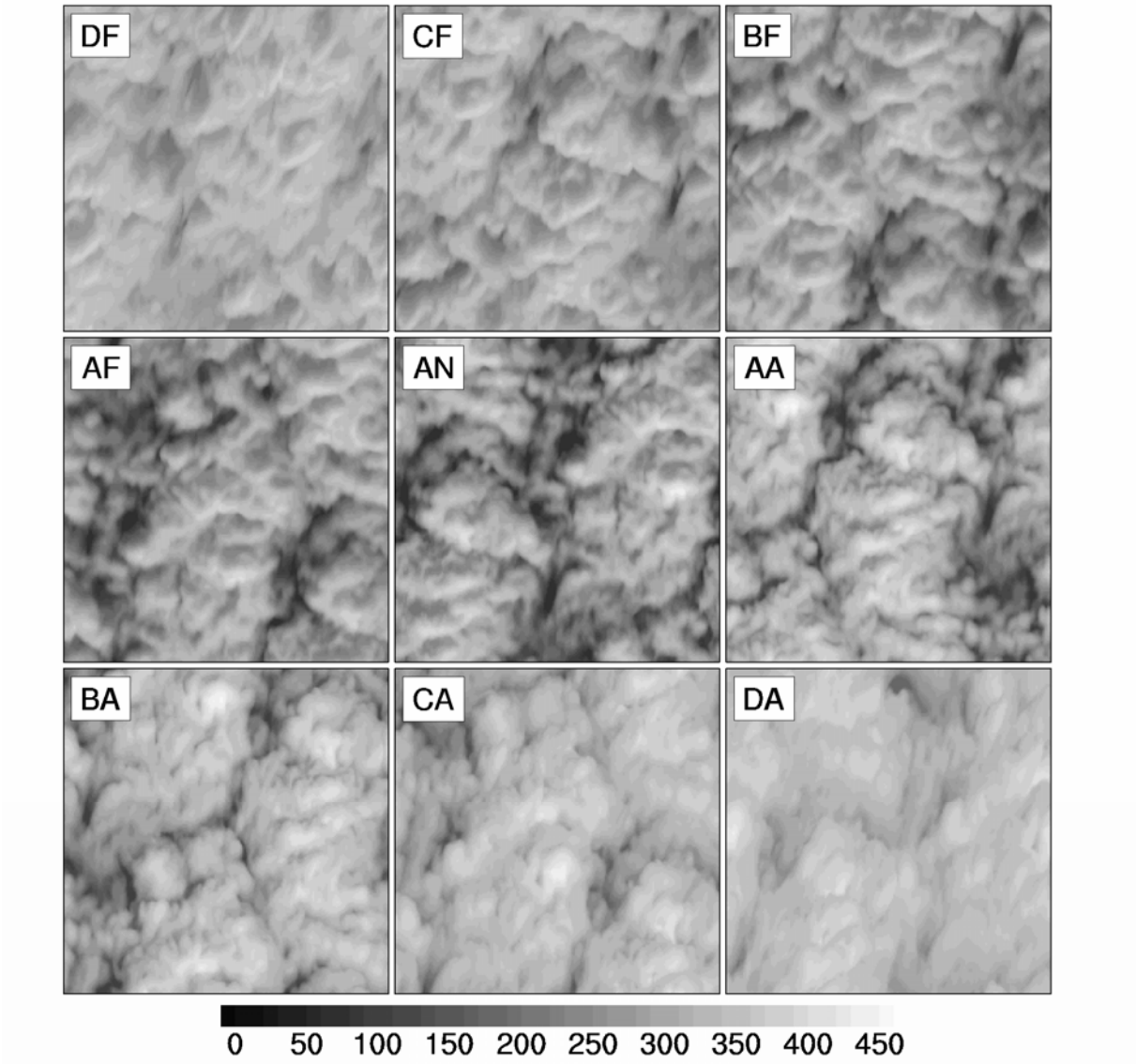

Figure 2. *Same as Figure 1 but for simulated radiances (W m^{-2} μm^{-1} sr^{-1}). Each panel consists of 200×200 pixels at 25 m resolution.*

The transition from cloud to clear air at near-nadir images appears to be sharp in the simulation and more subtle in observations. Simulations show smaller fraction of pixels with small radiances compared to the AirMISR. Analysis of histograms (not shown) indicates that the observed radiance distributions for these angles are more symmetrical than the modeled ones, which are skewed toward the larger values (Ovtchinnikov and Marchand, 2006). At off nadir angles, the model captures well both the shape and position of narrower distributions.

Figure 3a illustrates the angular dependence of the mean radiance. It quantifies the visual observation from figures 1 and 2 that the simulated clouds are brighter than the real ones at near nadir angles. The model and observations both show a minimum in the mean radiance at the AF and AN view angles, but the model overestimate the reflectance at these view angles. The increased reflectance at larger viewing angles compared to nadir (AN camera) is driven primarily by growing cloud optical path, which for plane parallel clouds is proportional to 1/cos(ξ), where ξ is the zenith viewing angle and by narrowing of the LWP distribution. The asymmetry in the angular distribution of the mean radiance about the AN view is the result of a minimum in the phase function, which for small droplets is located near 105° or between scattering angles corresponding to BF and AF directions (figure 4).

The variability of the fields represented by the standard deviation of radiance distributions decreases from its maximum at nadir view angle toward much smaller values at larger view angles (figure 3b), at which breaks in the cloud fields are closed by the cloud sides. The model distributions have slightly larger standard deviations and therefore are wider than the observed ones, particularly at the oblique angles (D cameras).

Changes in the symmetry of the distributions, as measured by their skewnesses, are illustrated in figure 3c. As with the means, the tendency of angular dependence is captured by the model, but the magnitude of change is underestimated, primarily because simulated clouds have sharper boundaries. Consequently, there are fewer and smaller areas of low reflectance in the simulated radiance field.

5. DISCUSSION

There are uncertainties in RT calculations related to the effects of underlying surface and vertical aerosol distribution. However, given the large cloud fraction, low surface albedo (0.04), and low aerosol optical depth (~ 0.1), the uncertainties in these factors are not nearly large enough to explain the observed differences. Positive model bias in the domain mean radiance at nadir indicates that the model may contain more condensate than the real cloud layer. However, the domain mean vertical liquid water paths (LWPs) of 106±57 g m^{-2} compares favorably with the MWR retrieval at the time of the overpath of 107±50 g m^{-2}. Model overestimation of the mean reflectance is more likely to be due to prediction of a too narrow distribution of the LWP. A future study should determine if the LWP and cloud top height distributions can be improved with refinement of the grid size below 25, and whether these improvements will lead to better representation of radiance angular dependence.

Another factor contributing to the model biases could be that the droplet effective radius near the cloud exceeds the cloud mean value of 6.8 used in the radiation transfer calculation. Increasing the effective radius would decrease the mean reflectance, more so for smaller optical paths, i.e., for smaller zenith viewing angles, thus resulting in stronger angular dependence.

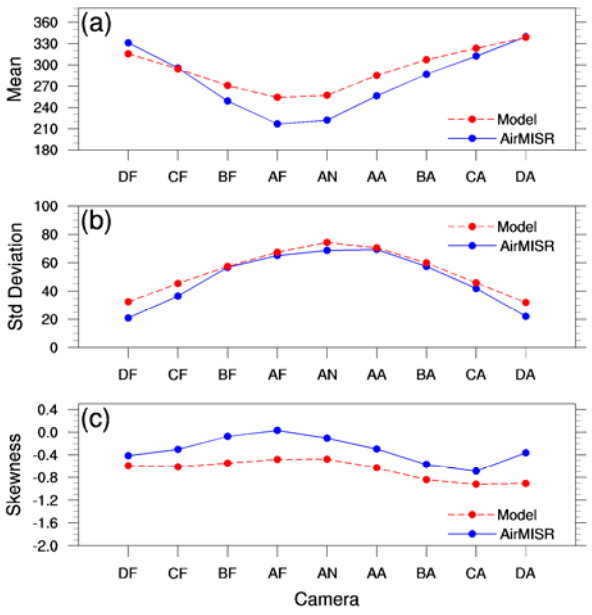

Figure 3. *Means (W m^{-2} μm^{-1} sr^{-1}), standard deviations (W m^{-2} μm^{-1} sr^{-1}), and skewnesses for the observed and simulated radiance distributions from figures 1 and 2, respectively.*

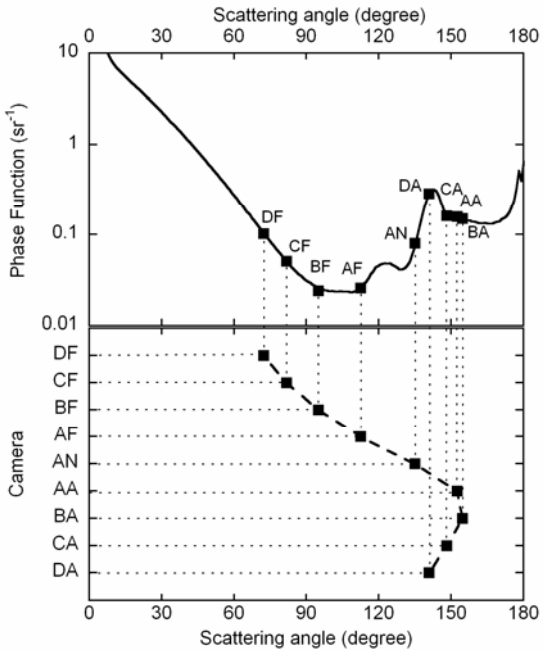

Figure 4. *Scattering angles for nine AirMISR cameras (lower panel) and corresponding values of a droplet phase function (upper panel).*

6. ACKNOWLEDGEMENTS

This study was supported by NASA through the Radiation Sciences Program. The AirMISR data were obtained from the NASA Langley Research Center Atmospheric Sciences Data Center. Other observations were obtained from the ARM Program data archive maintained by the DOE. The Pacific Northwest National Laboratory is operated for the DOE by Battelle Memorial Institute under contract DE-AC06-76RLO 1830. We are grateful to Marat Khairoutdinov and Frank Evans for providing the CRM and SHDOM codes, respectively.

7. REFERENCES

Khairoutdinov, M. F., and Randall, D. A., 2003: Cloud resolving modeling of the ARM summer 1997 IOP: model formulation, results, uncertainties, and sensitivities. *J. Atmos. Sci.*, 60, 607-625.

Diner, D., et al. (2005), The value of multiangle measurements for retrieving structurally and radiatively consistent properties of clouds, aerosols, and surfaces. *Remote Sens. Environ.*, 97, 495-518.

Evans, K. F. (1998), The spherical harmonics discrete ordinate method for three-dimensional atmospheric radiative transfer. *J. Atmos. Sci.*, 55, 429-446.

Ovtchinnikov, M., and R. Marchand, 2006: Cloud model evaluation using radiometric measurements from the airborne multiangle imaging spectroradiometer (AirMISR). *Remote Sens. Environ.*, (submitted).

Xie , S. C., et al. (2005), Simulations of midlatitude frontal clouds by single-column and cloud-resolving models during the Atmospheric Radiation Measurement March 2000 cloud intensive observational period. *J. Geophys. Res.*, 110, D15S03, doi: 10.1029/2004JD005119.